Wind and Structures, *Vol. 30, No. 1 (2020) 1-13*
DOI: https://doi.org/10.12989/was.2020.30.1.001

An engineering-based assessment methodology on the loss of residential buildings under wind hazard

Mingxin Li[a] and Guoxin Wang*

State Key Laboratory of Coastal and Offshore Engineering, Dalian University of Technology, Dalian 116024, China

(Received December 17, 2018, Revised June 23, 2019, Accepted August 7, 2019)

Abstract. The loss prediction and assessment during extreme events such as wind hazards is always crucial for the group low-rise residential buildings. This paper analyses the effect of variation in building density on wind-induced loss for low-rise buildings and proposes a loss assessment method consequently. It is based on the damage matrices of the building envelope structures and the main load-bearing structure, which includes the influence factors such as structure type, preservation degree, building density, and interaction between different envelope components. Accordingly, based on field investigation and engineering experience, this study establishes a relevant building direct economic loss assessment model. Finally, the authors develop the Typhoon Disaster Management System to apply this loss assessment methodology to practice.

Keywords: wind hazard; loss assessment; residential buildings; Monte Carlo; ArcGIS

1. Introduction

Research on the wind resistance of low-rise buildings has always been of immediate practical significance, especially for the severely affected rural regions in southeastern China. Due to the defects in the design and construction, the wind-resistance performance of rural buildings is reduced as provided in previous wind events. Therefore, almost every wind disaster can bring severe losses to the residential buildings in this area.

Currently, research on the interaction between building structure and wind is more focused on the wind-induced response of high-rise structures. Wang *et al.* (2016) investigated the wind loads of the large billboard structures with two-plate and three-plate configuration by the wind tunnel. Lin *et al.* (2017) proposed a method for calculating the stochastic wind field based on cross stochastic Fourier spectrum. Huang and Gu (2018) developed a simplified three-dimensional calculation model for the dynamic analysis of soil-pile group-supertall building systems excited by wind loads using the substructure method. There are also some research focused on wind pressure changes caused by changes in the shape of low-rise buildings, see in Wang and Li (2015) and Feng *et al.* (2018).

The development to assess the wind-induced loss of residential buildings can be mainly divided into two phases.

The earlier methods were focused on the regression analysis on the claim data collected by insurance companies. Mitsuta *et al.* (1996) analyzed the relationship between insurance claim figures and wind speed for Typhoons Mirelle. A similar analysis for Hurricane Andrew can be found in Bhinderwala (1995). However, those regression and empirical models are specific to the observed structures and regions, and the applicability to other structures and locations may require more modification. Also, they are limited by post-disaster statistics.

Recently, engineering principles are utilized to project physical damage based on the knowledge of wind-structure interaction and component capacities. Compared with the previous regression models, these models are designed to predict physical damage based on the performance and resistance of various buildings components and their interaction under wind loads (Pita *et al*. 2013).

Pinelli *et al.* (2004) proposed a hurricane damage prediction model for residential structures, where a single masonry structure was taken as an example to analyze the possible damage during a hurricane. Vickery *et al.* (2006) analyzed the building envelope and interior damage under hurricane, which has been applied to the public model, HAZUS-MH Hurricane Model (FEMA 2017). Monte Carlo simulations are utilized in the Florida Public Hurricane Loss Model (FPHLM), which includes an engineering model to assess the exterior damage (Pinelli *et al.* 2008). Long (2008) proposed a typhoon disaster investigation and evaluation method for local buildings based on engineering experience judgment, which can judge the failure form of structural components and the corresponding damage level standard. However, it didn’t form a comprehensive evaluation standard for the damaged building. Liu (2016) carried on finite element simulation on the performance of the main load-bearing structure of a masonry building at various wind speeds. The maximum interlayer displacement angle and vertex displacement for the masonry building were taken as the evaluation indicators to analyze the damage quantitatively and qualitatively. Zhong *et al.* (2017) evaluated the damage state of masonry buildings by taking

*Corresponding author, Professor
E-mail: gxwang@dlut.edu.cn
[a]Ph.D.
E-mail: jiexia1991@mail.dlut.edu.cn

http://www.techno-press.org/?journal=was&subpage=7 ISSN: 1226-6116 (Print), 1598-6225 (Online)

the roof tiles and walls as the main evaluation indicatior.

Moreover, some loss assessment models include the various changes in wind pressure and the impact loss from wind-induced debris in wind hazard. Zhang *et al.* (2014) developed a reliability-based vulnerability model for the assessment of typhoon-induced wind risk of residential buildings in Japan. Peng *et al.* (2016) proposed an engineering-based tornado damage assessment (ETDA) model, then validated this model using four damaged buildings in 2011, Joplin, MO, tornado.

In this study, an integrated assessment model with quantified assessment criteria is developed. Combined with the analysis on the envelope structure of low-rise residential buildings under fierce winds, the effects of wind speed, wind direction, wind-induced interference effect, building density, structure type, and structural preservation degree are taken into consideration for this model. Besides, the corresponding building economic loss model is deduced in this paper. Finally, the integrated loss assessment model is applied to self-developed Typhoon Disaster Management System, which can assist with wind disaster conveniently.

2. Effect of variation in building density on wind-induced loss for low-rise buildings

The building group and arrangement are shown in Fig. 1. Based on the characteristics of typical gable roof masonry buildings in southeastern China, this building group (including nine identical buildings with the same size, Fig. 1(b)) are modeled by MATLAB in this simulation. Basswood is chosen as the material of roof panel (1.2 m × 1.8 m × 10 mm), which has a density of 500 kg/m^3. The standard flat tile (Fig. 4) is chosen as the roof tile with a weight of 5.2 kg and a size of 0.332 m × 0.42 m. So, according to the roof size, 32 roof panels can be placed on each side of the roof, and 20 roof tiles can be placed on each roof panel. The size of the window and the door is 1.8 m × 1.5 m, 1.5 m × 2 m respectively. It is worth mentioning that the buildings group are arranged symmetrically and neatly in this simulation, which is common in the planned and designed rural buildings, so the simulation results may not be applicable to the complex and messily arranged buildings.

To study the effect of variation in building density (CA) on the wind-induced loss of buildings group, three kinds of building density are analyzed during this simulation, which is consistent with the wind tunnel measured data in TPU (2007). The calculation process of CA for buildings group can be found in Fig. 1(a).

Similarly, ten directions from 0° to 90° with an increment of 10°and eight wind speeds from 15 m/s to 50 m/s with an increment of 5 m/s at 10 m height are simulated totally. Besides, simple harmonic superposition method is utilized to simulate the Davenport spectrum, and the non-Gaussian properties of wind speed are not considered in this study. Therefore, if there is a higher accuracy need of wind speed simulation, the related simulation method of non-Gaussian wind effects can be found in Masters and Gurley (2003) Peng *et al.* (2014) and Yang and Gurley (2015). To

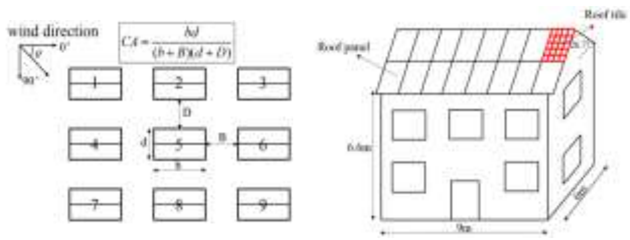

(a) Buildings group arrangement

(b) Building size

Fig. 1 Low-rise residential building group

Table 1 Various building density

Building density (CA)	0.1	0.3	0.6
B [m]	12	5	1.8
D [m]	21	7.5	2.7

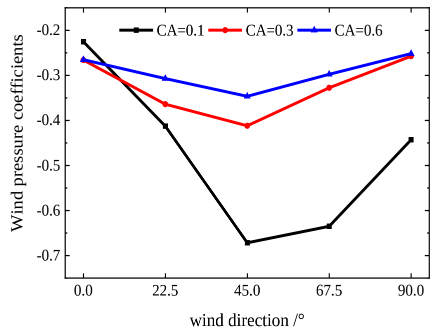

Fig. 2 The change of mean values of wind pressure coefficients on the gable roof

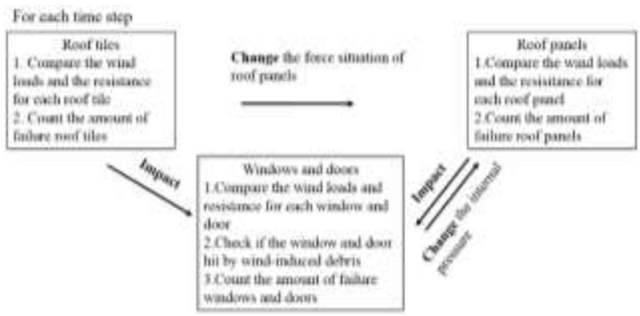

Fig. 3 The calculation process of each time step during the Monte Carlo simulation

Fig. 4 The forces status of a roof tile

balance the need for results accuracy and calculation (3 * 8 * 10 = 240 work conditions), each wind load condition is simulated 50 times by Monte Carlo method.

The difference between this part and previous work in Li and Wang (2018) is mainly the change of wind pressure coefficients values for each building density. After wind tunnel test data (TPU 2007) processing, the change of mean values of wind pressure coefficients on the roof surface along with wind directions for each building density is shown in Fig. 2.

The wind-induced failure model of three component (roof tiles, roof panels, windows and doors) is established based on their physical properties, local geomorphic features, and the mechanisms of interaction. The interaction between different components concludes: a) The failure roof tiles can impact the doors and windows of surrounding houses, and also change the situation of the forces of roof panels; b) The failure roof panels can impact the windows and doors of surrounding buildings; c) The failure of doors and windows will change the internal pressure of the building. Finally, the calculation process of each time step during this simulation is shown in Fig. 3.

2.1 Roof tiles

There are many types of roof tiles for the rural buildings in China, and the construction quality varies greatly. In some areas, the roof tiles are connected to the roof structure by mortar or nails. In this paper, the roof tile model is more common and also has poor construction quality. Without any mortar and nail, the roof tiles are placed directly on the roof structure (Fig. 4). In this paper, under the pressure from adjacent roof tiles and the friction between the roof tile and the roof structure, the roof tile will not slip. The connection between adjacent roof tiles is such that the upper and lower quarters of the tile are overlapped, and the left and right sides are snapped together. The failure of a roof tile is assumed to occur when the wind suction load L_t exceeds the resistance, which consists of the gravity force G_t and the pressure from adjacent roof tiles R_{tp}, shown as follows.

The failure model of a roof tile can be written as

$$L_t - (R_{tp} + G_{t'}) > 0 \tag{1}$$

where $G_{t'}$ is the component of the roof tile gravity in the normal direction of the roof.

As the outermost component, the roof tiles always fail earlier compared with other components. To analyze the failure roof tiles, this paper defines a variable: the cumulative average loss of roof tile, CM_{RT}. By adding the cumulative amount of failure roof tiles after each simulation and then divided by the total number (50) of simulations, the value of CM_{RT} can be obtained. The variation of CM_{RT} for each building density is shown as follows.

Fig. 5 shows that the smaller the building density is, the larger the CM_{RT} values are, especially for the wind speed $v \leq 30$ m/s. However, this phenomenon is no longer apparent for wind speed v > 35 m/s. For the wind direction interval of 30°-90°, due to the higher values of wind pressure coefficients, the CM_{RT} values for CA = 0.1 have much larger values than the CM_{RT} values for CA = 0.3 and CA = 0.6.

Besides, for the wind speed v = 30 m/s, it has greater value for CM_{RT} in CA = 0.6 than CA = 0.3, especially for the wind direction from 50° to 90°. However, the mean wind pressure coefficients on the roof surface have similar values in CA = 0.3 and CA = 0.6, as shown in Fig. 2. After the wind pressure data processing for the wind direction of 90°, the frequency distribution histograms for CA = 0.3 and CA = 0.6 are shown in Fig. 6. The amount of wind pressure measuring points that have the pressure coefficients greater than -0.23 are occupied a lower proportion for CA = 0.3, while it is opposite for CA = 0.6. Therefore, compared with CA = 0.3, it will bear higher wind suction loads for the roof tiles in CA = 0.6, which leads to higher values for the CM_{RT}.

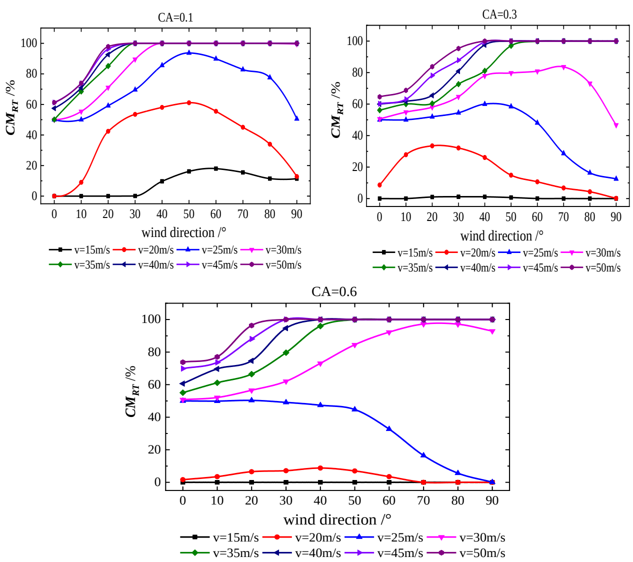

Fig. 5 The variation of CM_{RT} with wind direction and building density

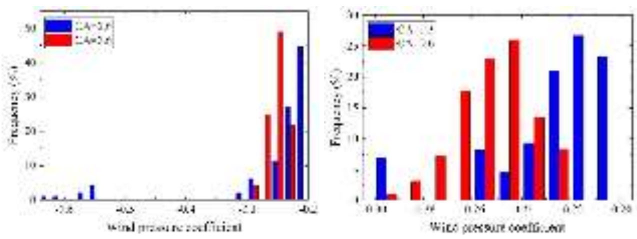

(a) Wind pressure coefficients interval of -0.65 ~ -0.2

(b) Wind pressure coefficients interval of -0.3 ~ -0.2

Fig. 6 The frequency distribution of wind pressure for CA = 0.3 and CA = 0.6

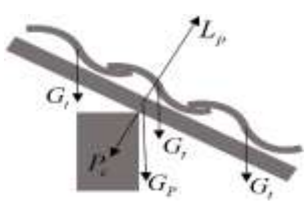

Fig. 7 The forces status of a roof panel

Table 2 The maximum values of CM_{RP} for the wind speed of 30 m/s and 35 m/s

Maximum value of CM_{RP} (%)			
CA	0.1	0.3	0.6
v = 30 m/s	13.5	0.5	0
v = 35 m/s	49	18.9	6.7

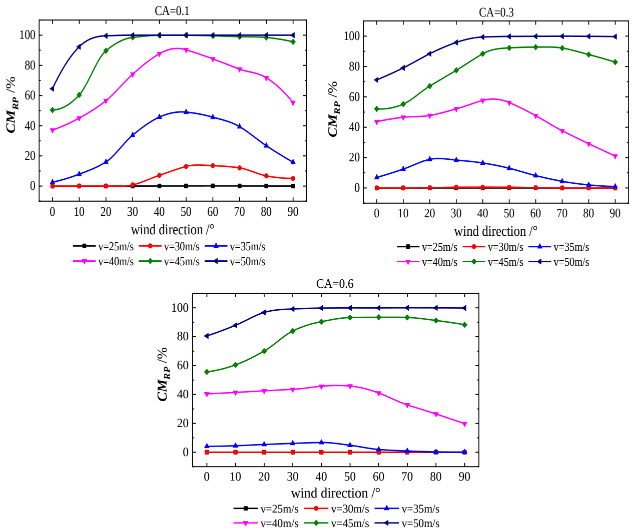

Fig. 8 The variation of the CM_{RP} with wind direction and building density

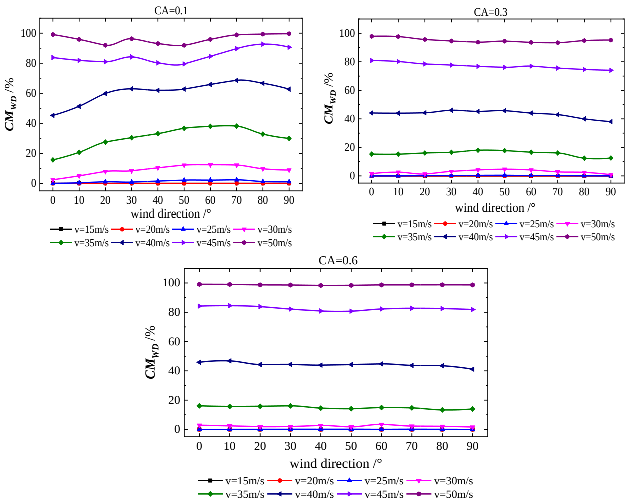

Fig. 9 The variation of the CM_{WD} with wind direction and building density

2.3 Windows and doors

The failure model of windows and doors can be generalized to three models: 1) Failure by wind pressure action; 2) Failure by the impact from roof tiles debris; 3) Failure by the impact from roof panels debris.

2.3.1 Failure by wind pressure action

Alike with the two previous components, the failure model of window and door under wind pressure can be written as

$$L_w - R_w > 0 \tag{3}$$

where L_w and R_w are the wind pressure and wind resistance of windows or doors respectively.

Similarly, the cumulative average loss of windows and doors for all buildings, CM_{WD}, is defined here. After the data processing of the loss of windows and doors failed by wind pressure action, the variation of CM_{WD} for the group residential buildings in different conditions is shown in Fig. 9.

It indicates that the CM_{WD} values increase as wind speed increases. And it also proves that CM_{WD} has similar values between CA = 0.3 and CA = 0.6 for most wind directions,

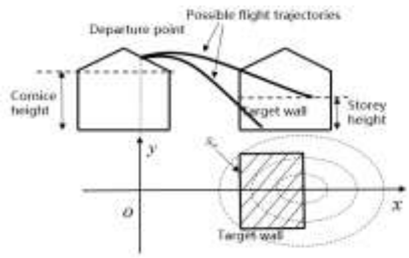

Fig. 10 The mechanism of roof tiles debris impacting windows

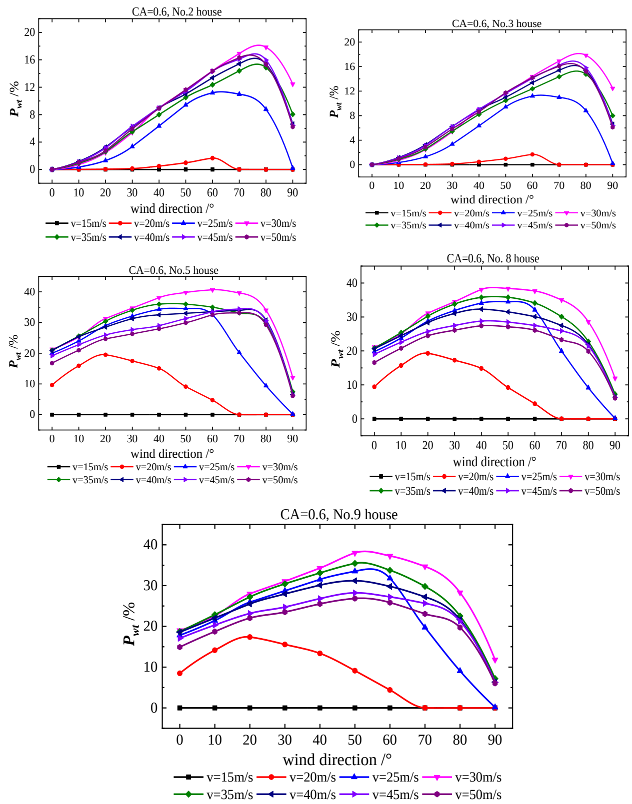

Fig. 11 The variation of P_{wt} with wind direction for CA = 0.6

whereas the CM_{WD} have higher values for CA = 0.1 in some cases. Besides, the variation of CM_{WD} under different wind directions is not obvious, especially for CA = 0.3 and 0.6, and the CM_{WD} have less variation to wind direction for the greater building density. That is due to the small change of the wind pressure coefficients on windows and doors in the change of wind direction (TPU 2007).

2.3.2 Failure by the impact of roof tiles debris

The damaged roof tiles will fly around under the fierce wind action, and some of them can impact the windows of surrounding buildings. The mechanism of the impact process is rough as Fig. 10.

During the flying of failed roof tiles under the wind suction, it is assumed that only the windows on the windward wall may be hit. The shaded area (S_m) is the projection of the windward wall on the ground, and it is a parallelogram. The dotted elliptical area is the possible landing regions of the failed roof tiles. The flying trajectory of a roof tile is modeled taking a basis on the research of Lin and Vanmarcke (2010), and the probability density function $\boldsymbol{\mu(x,y)}$ of landing positions for the flying roof tiles can be expressed as

$$\mu(x,y)=1/(2\pi\sigma_x\sigma_y)\cdot\exp\left[-1/2\left\{((x-m_x)/\sigma_x)^2+(y/\sigma_y)^2\right\}\right] \tag{4}$$

A total of 5 buildings, No. 2, No. 3, No. 5, No. 8 and No. 9, are taken as the research targets during the calculation of the probability of windows impacted by roof tiles (P_{wt}) debris from surrounding buildings. Due to limited space, only the variation of P_{wt} with wind direction for CA = 0.6 is shown in Fig. 11.

During the variation of the wind direction from 0° to 90°, the research target building of No. 2 and No. 3 are almost always in the upstream of the wind fluid, so the P_{wt} values of these two buildings are always lower for most wind directions. Further, because of the similar source buildings for roof tiles debris, P_{wt} has similar values for No. 2 and No. 3 buildings. Similarly, the relationship between the P_{wt} values of No. 8 and No. 9 buildings can be explained as such.

Several characteristics illustrated in Fig. 11 are also worth mentioning. For example, the wind speed led to the greatest value of P_{wt} is not the highest wind speed of 50 m/s, but 30 m/s. When the wind speed reaches a higher value, the mean distance between the landingpositions of roof tiles debris and the target building become farther and farther, which reduced the probability of windows impacted by roof tiles debris.

It is also observed that for a wind speed of 25 m/s, P_{wt} reduces significantly when the wind direction is close to 90°. It can be explained that the CM_{RT} values reduce significantly from the wind direction of 60° to 90° for CA = 0.6 (Fig. 5), which will reduce the probability of windows impacted by roof tiles debris.

Besides, compared with other research target buildings, No. 5 building has the highest value of P_{wt}, which is related that the windows of No. 5 building have the most amount of source buildings for roof tiles debris. Therefore, the order of buildings according to the value of P_{wt} from high to low is No. 5, No. 6 & No. 8 & No. 9, No. 2 & No. 3 & No. 4 & No. 7, No. 1.

Next, limit to space, this study only selects the related results of No. 2, No. 5 and No. 8 buildings to reveal the variation of P_{wt} with building density, as shown in Fig. 12.

It is observed that the greater the building density, the higher the P_{wt} values. For example, the maximum P_{wt} value of No. 5 building is 19.8% for CA = 0.1, while the related values are 25.5% and 40.6% respectively for CA = 0.3 and CA = 0.6. In Fig. 5, when the building density increases, the loss of failure roof tiles will decrease, but the distance between adjacent buildings will decrease as well, which will lead to the easier impact by roof tiles debris for the windows of target buildings.

2.3.3 Failure by the impact from roof panels debris

The loss of windows impacted by roof panels debris cannot be ignored either. Compared with the Section 2.3.2, the failure model of windows impacted by roof panels is more accurate due to the small number of roof panels. In the flight, there are three forces acting on a roof panel debris, shown in Fig. 13, which takes a basis on the flat plate trajectory proposed by Tachikawa (1983).

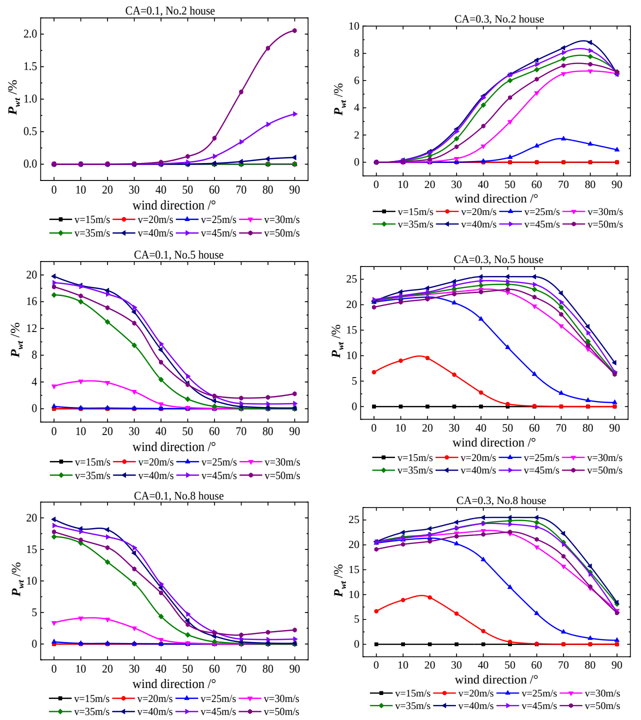

Fig. 12 The variation of P_{wt} values with building density for No. 2, No. 5 and No. 8 buildings

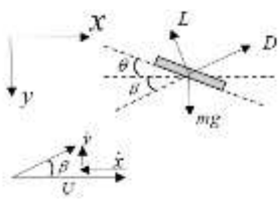

Fig. 13 Forces acting on a roof panel in the uniform flow, see in Dao *et al.* (2012)

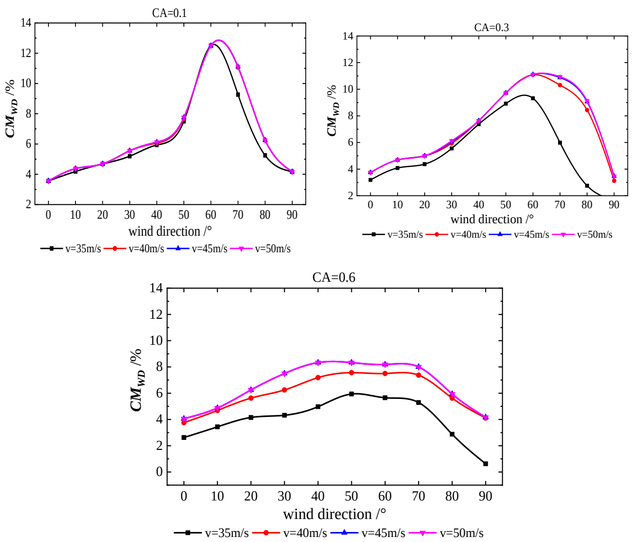

Fig. 14 The variation of CM_{WD} under the impact from roof panel debris

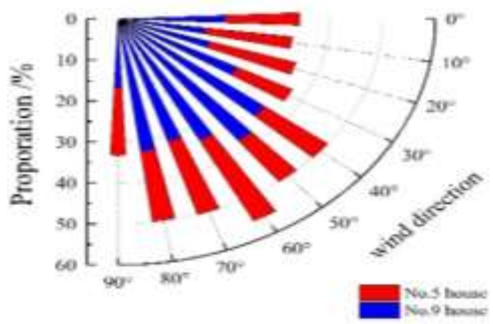

Fig. 15 The proportion of the CM_{WD} values of No. 5 and No. 9 buildings in the group impacted by roof panels debris for CA=0.1

For a flying roof panel, D is the drag force, L is the lift force and mg is the gravity. x and y are the coordinates which indicate the location of the roof panel. Θ is the angle between the roof panel and the horizontal direction. β is the angle between the roof panel and the direction of relative wind speed (U- $\dot{x}$) for the roof panel.

The force analysis for a roof panel in the flight can be expressed as

$$
\begin{aligned}
m\ddot{x} &= \frac{1}{2}\rho A\left[(U-\dot{x})^2+\dot{y}^2\right]\left(C_D\cos\beta-(C_L+C_{LA})\sin\beta\right)\\
m\ddot{y} &= mg-\frac{1}{2}\rho A\left[(U-\dot{x})^2+\dot{y}^2\right]\left(C_D\sin\beta-(C_L+C_{LA})\cos\beta\right)\\
I\ddot{\theta} &= \frac{1}{2}Al\left[(U-\dot{x})^2+\dot{y}^2\right]\left(C_M+C_{MA}\right)
\end{aligned}
\tag{5}
$$

where ρ is the air density, g is the acceleration of gravity, A, m, l and I are the area, mass, chord length and moment of inertia of the roof panel respectively. $B = tan[\dot{Y}/(U-\dot{x})]$ and a dot means the derivate with respect to time t. C_D, C_L and C_M are the drag, lift and moment coefficients respectively.

Fig. 14 shows the variation of CM_{WD} values with wind direction and building density, for those lower wind speeds ($v \le 30$ m/s), CM_{WD} are not shown here because their values are small enough to ignore.

It is evident that the CM_{WD} values decrease with the increase of building density, which is opposite to the failure of windows impacted by roof tiles debris. Because the farther flying distance of roof panels debris, the distance between adjacent buildings may be more suitable for the windows impacted by roof panels debris in CA = 0.1 and CA = 0.3. Furthermore, the target buildings have a small number of windows on the along-wind directions for wind direction of 0° and 90°, which leads to the lower CM_{WD} values in these two directions.

In addition, the effect of changes in building location on the windows impacted by failure roof panels is analyzed in this part. In the process of wind direction change from 0° to 90°, only the doors and windows of 8 houses are likely to be hit by the failed roof panels, i.e., No. 2 to No. 9 buildings.

Fig. 15 shows the proportion of CM_{WD} values of No. 5 and No. 9 buildings to the total CM_{WD} values of buildings group for CA = 0.1. The sum proportion can be defined as $P_{5,9}$ as follows:

$$
P_{5,9}=\frac{CM_{WD}(5)+CM_{WD}(9)}{\sum_{i=2}^{9}CM_{WD}(i)}
\tag{6}
$$

Where $CM_{WD}(i)$ is the CM_{WD} value of No. I building impacted by failed roof panels. Due to the limitation of space, the related statistics of other buildings are not shown here. It can be found that $P_{5,9}$ is greater than 30% for all wind directions, and it is even greater than 50% from the wind direction of 40° to 80°. That proves the doors and windows of those buildings located in the middle and

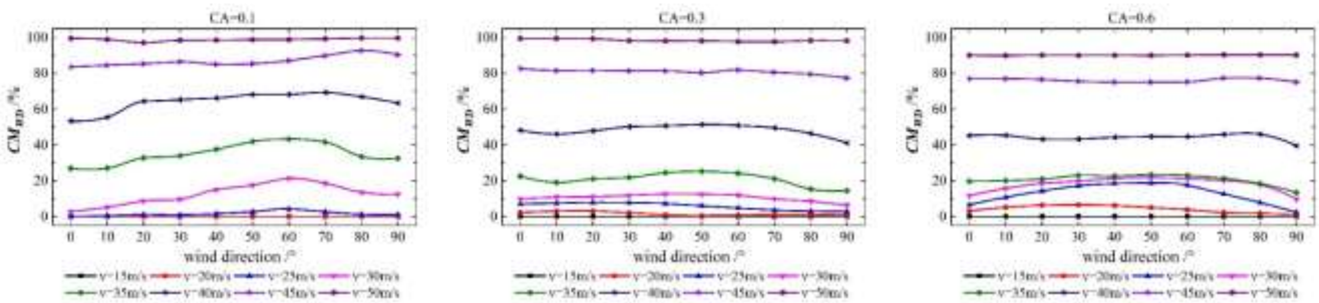

Fig. 16 The unified CM_{WD} of the buildings group for different building densities

downstream of the wind are more vulnerable to be impacted by the flying roof panels debris.

2.3.4 United failure model for windows and doors

Based on the simulation results in Section 2.3.1-2.3.3, Fig. 16 shows the variation of unified CM_{WD} for this buildings group with wind direction and building density. The variation of CM_{WD} is affected obviously by the change of wind direction for the lower wind speeds ($v \le 30$ m/s). It can be explained that the CM_{WD} values are mainly affected by the impact of wind-borne debris for such wind speeds. For the higher wind speeds ($v \ge 35$ m/s), it has an opposite performance, which means the wind pressure action would be the main reason that made the windows damaged when the wind speed reaches a higher stage.

3. Damage model of group residential buildings under wind disaster

It is common knowledge that residential buildings in various regions are quite different in the shape, structure type and materials. Therefore, in order to propose a general wind-induced loss assessment model, this paper divides the evaluation object of the structure into two parts: the envelope structure and the main load-bearing structure. As the envelope structure is more vulnerable to damage during windstorms and its losses are more serious, the loss assessment of the envelope structure should be more detailed.

In the previous section, based on the Monte Carlo simulation, the physical properties, building density, the interaction between different components, and other influencing factors of the envelope structure (roof tiles, roof panels, windows and doors) are considered during the wind disaster. The results will constitute the damage matrix of the envelope structure in this paper.

Therefore, for this study, the failure of envelope components of group residential building can be obtained by a three-dimensional matrix (n×m×k) including wind speed, wind direction, and building density, where n = 8, representing eight kinds of wind speeds, m = 10, representing ten wind directions, k = 3, representing three building densities. Any element in the damage matrix can be expressed as aswd, where s represents different wind speeds, w represents different wind directions, and d represents different building densities.

For the main load-bearing structure, the loss assessment model is more simplified. The influence factors contain structure type and preservation degree, shown in Eq. (7). Furthermore, combined with the research results in Liu (2016) and Zhong *et al.* (2017), the failure probability of the main load-bearing structure can be obtained as follows:

$$P=P_{m,w} \cdot C_s \cdot C_{pd} \tag{7}$$

where P is the failure probability of the main load-bearing structure, $P_{m,w}$ is the failure probability of the masonry structure with weak preservation. C_s and C_{pd} are the influence coefficients of structure type and preservation degree on the failure probability of the main load-bearing structure respectively.

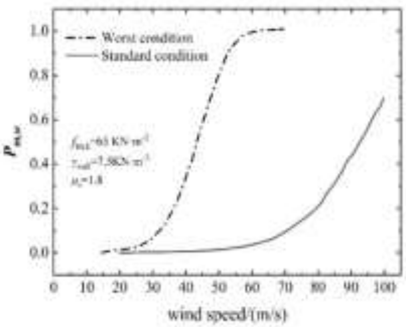

Fig. 17 Vulnerability of walls for masonry building under the most unfavorable conditions

Table 3 Brief characteristics of structure type

Structure type	Characteristics	C_s
Masonry	It mainly divided into brick masonry and stone masonry structure. Most of them contain wooden gable trusses. The wall is the main load-bearing structure, without ring beams, and the floor slabs are directly placed on the cross wall with poor integrity. Most of them were built before the 1990s.	1
Brick-concrete	The vertical load-bearing structure is brick wall/block. The ring beam, floor, and structural column are reinforced concrete. The main load-bearing structure is the floor and wall. The number of layers is generally less than 6. Most of them were built after the 1990s.	0.72
Frame	The main load-bearing structure mainly consists of beams, slabs and columns, and it has good integrity and rigidity. More of them were built after 2000.	0.35

Based on Monte Carlo simulation, the failure probability of main load-bearing structure of rural masonry structure buildings under the worst condition (the worst construction quality, the worst material quality, and the most unfavorable wind load shape coefficient) was obtained in Zhong *et al.* (2017). The result (Fig. 17) will be the main base for the value of $P_{m,w}$ in Eq. (7).

According to the field research on the buildings in Yunmei Village (Fig. 18) and the reference to wind disaster investigation (Huang *et al*, 2010), there are mainly three types of low-rise residential structures commonly found in southeastern China: masonry structure, brick-concrete structure, and frame structure. During wind disaster, the influence of the structural type on the wind-resistance of the main load-bearing structure is difficult to estimate quantitatively. Huang *et al.* (2010) surveyed the wind resistance of rural houses in coastal areas of Zhejiang Province and counted the damage of more than 5,000 houses after the typhoon of Saomai. In this paper, the wind resistance of different structural types in the survey results is normalized, and the influence coefficient of the structure type, Cs, on the wind resistance capacity of the main load-bearing structure is obtained based on the masonry structure, as shown in Table 3.

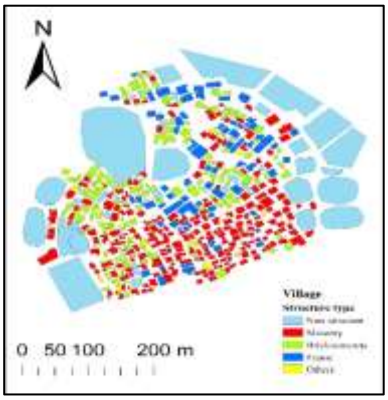

Fig. 18 Structure type distribution in Yunmei village

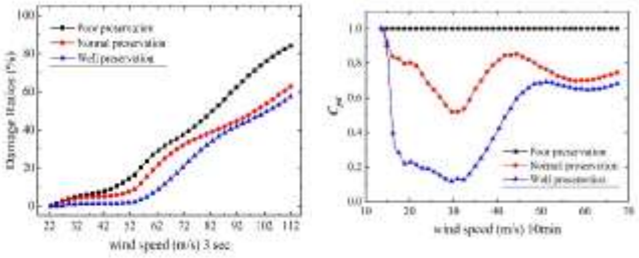

(a) Vulnerability curves (b) Influence coefficients

Fig. 19 Influence coefficients of preservation degree on wind resistance

Besides, another influencing factor is the preservation degree. Based on the construction quality, construction age, and preservation status, it is divided into three categories: well preservation, normal preservation, and poor preservation. Well preservation represents the strongest wind resistance for the main load-bearing structure, and poor preservation is the opposite. Due to the high complexity and difficulty, there is currently little quantitative research about the influence of preservation degree on wind resistance for low-rise buildings. Based on the wind resistance analysis of masonry buildings with different characteristics (Pinelli *et al*. 2008, 2011), Fig. 19 shows the wind resistance of masonry buildings with different characteristics. The damage ratio value in each state in Fig. 19(a) is divided by the damage ratio value in the state of poor preservation, and the Cpd value Fig. 19(b) in each preservation state can be obtained.

In Fig. 19(a), the structural characteristics that affect the wind resistance of the structure are related to the construction quality, and its application to Chinese construction is still needed to be discussed, especially in term of preservation degree. If there is a more appropriate and realistic relevant research in the future, then the Cpd coefficient in Eq. (7) needs to be re-valued.

Similarly, the failure probability of the main load-bearing structure can also be obtained through a three-dimensional matrix (n × j × b) containing wind speed, structure type, and structural preservation integrity, where n = 8, representing eight wind speeds, j = 3, representing three structural types, b = 3, representing three preservation degrees. Any element of this damage matrix can be expressed as bstp, where s represents different wind speeds, t represents different structural types, and p represents different preservation degrees.

4. Direct economic losses

After the wind disaster passed, the direct economic loss of each building refers to the construction price required to repair the damaged house and restore the same scale and standard before the disaster based on the current price. The direct economic loss of the building can be broken down into the replacement cost of each component

$$C = D \cdot C_R \cdot V \tag{8}$$

where C is the base cost to repair the component, D is the fraction of the component to be replaced or repaired, C_R is the cost ratio for the component, and V is the building value.

Affected by factors such as region, architectural style, structure type, etc., it is difficult to give a unified estimate of the unit cost of the buildings and the specific cost ratio of each component. Through field investigation and combined with the wind disaster investigation in southeastern China (Huang *et al*. 2010), the average cost of low-rise houses in the coastal areas and the cost of each component are as shown below.

In Table 5, interiors include installation works, water, electricity, and heating works and so on, excluding property inside the house. In this model, the economic damage to the interior of the building is a function of the damage of envelope structure (Vickery *et al*. 2006). The basic premise used in the development of these simple models is that once the envelope is breached, most of the damage to the interior of the building is a function of the amount of water that enters the building.

$$\text{maximum}\begin{cases} L_{RC} = f_1(R_{RC})(1 - f_2(A_{RC}))\, f_3(R_{RC})V_I \\ L_s = (3.6R_s + 0.1)V_I + R_S V_{RF} \end{cases} \tag{9}$$

where L_{RC} and L_S are internal damage caused by failed roof tiles and roof panels respectively, R_{RC} is the fraction of failed roof tile, A_{RC} is the area of failed roof tiles, and V_I is the value of the interior of the building. R_S is the proportion of failed roof panels, and V_{RF} is the value of the roof framing. When the failure ratio of roof panels exceeds 0.25, the internal loss of the house can be considered to reach a maximum.

The function f_1 represents the fractional amount of the interior area affected by the loss of a fraction of the roof tiles.

$$\begin{cases} f_1(R_{RC}) = 1.11R_{RC} & (R_{RC} \le 0.9) \\ f_1(R_{RC}) = 1.0 & (R_{RC} > 0.9) \end{cases} \tag{10}$$

The function f_2 represents a term that accounts for the fact that when the amount of roof tiles damage is relatively small, in many cases water is not able to enter the building.

(a) v = 20 m/s

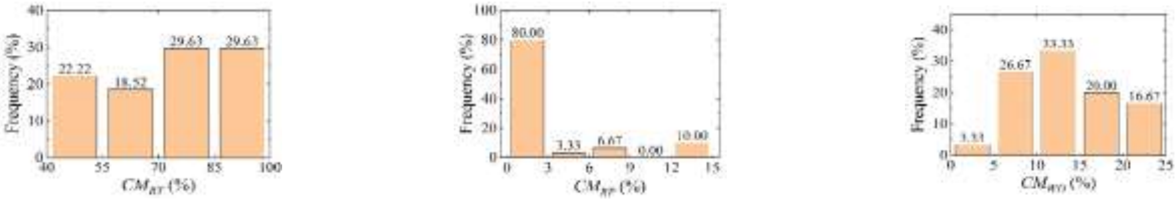

(b) v = 30 m/s

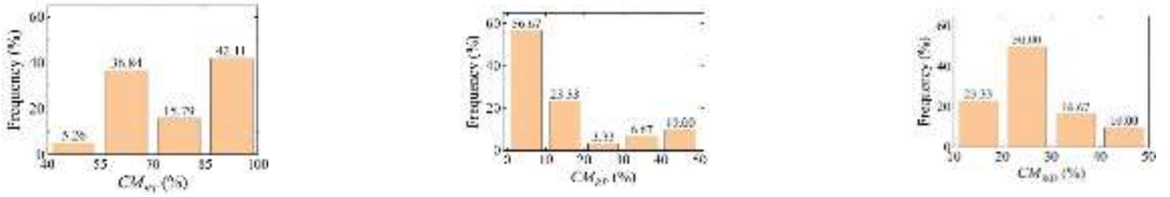

(c) v = 35 m/s

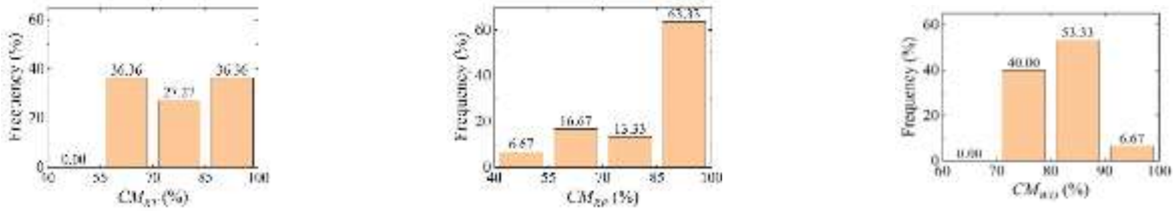

(d) v = 45 m/s

Fig. 20 Frequency distribution of failed envelope components at different wind speeds

$$\begin{cases} f_2(R_{RC}) = 1 - 0.005 A_{RC} & (A_{RC} \le 18.58 \text{ m}^2) \\ f_2(R_{RC}) = 0 & (A_{RC} > 18.58 \text{ m}^2) \end{cases} \tag{11}$$

The function f_3 represents a term that accounts for the fact the resulting interior economic damage becomes more severe as the area of interior damage becomes lager.

$$\begin{cases} f_3(R_{RC}) = 0.1 & (R_{RC} \le 0.05) \\ f_3(R_{RC}) = 2.0 R_{RC} & (0.05 < R_{RC} \le 0.5) \\ f_3(R_{RC}) = 1.0 & (R_{RC} > 0.5) \end{cases} \tag{12}$$

Similarly, due to the few research about the wind-induced loss of group low-rise buildings in China, this study draws on the more mature research in Vickery *et al.* (2006). Therefore, the applicability of the internal loss model to Chinese constructions still needs further study.

5. Loss assessment of damaged group residential buildings under wind disaster

During wind disaster, the loss assessment of damaged buildings can help the local government departments to grasp the damage extent of the building, classify the buildings with different damage level, and carry out corresponding post-disaster relief work. Therefore, the loss assessment of damaged residential buildings after the windstorm has important practical significance.

In this paper, the envelope components and main load-bearing structure of the damaged houses are graded to different extents, and then the overall loss assessment is formed. The evaluation factors of each damage level consist of the damage degree of each envelope component and the main bearing structure. Combined with the damage analysis of Section 2 and the damage model of the main load-bearing structure in Section 3, the damage states of the damaged buildings are divided into four levels: no/ very minor damage, minor damage, moderate damage, and severe damage.

First, determine the critical conditions between different damage states. In this paper, when the house is in no/very minor damage, the failure probability of the main load-bearing structure should be 0, and since the roof panel is more difficult to be damaged than other two envelope components, the damage of the roof panel is also 0. In addition, when the roof panel damage exceeds 25% and the roof tile damage exceeds 90%, the internal economic loss of the damaged house will reach a maximum value (Eqs. (9)-(12)), in that case, the damage level of the damaged building can be defined as severe damage. Therefore, combined with the damage performance at different wind speeds, v = 20 m/s, v = 30 m/s, v = 35 m/ and v = 45 m, which may be the critical wind speed values for different damage levels, are selected here for analysis.

Combined with the engineering practice, the principle of the failure interval of each component at different damage states is selected as follows: the probability that the damage ratio of the component exceeds the failure interval is not more than about 20%. For example, if the failure interval of the roof panel is assumed to be [10%, 30%] for the moderate damage, then the probability of damage ratio of roof panel higher than 30% is not more than about 20%. The failure frequency distribution of different envelope components under these four wind speeds is shown in Fig. 20. It can be seen that for v = 20 m/s, the frequency of the failed roof tile less than 35% is close to 80%, and the frequency of the failed doors and windows less than 5% is 83%. At this time, the roof panel and the main load-bearing structure are no damaged, so the damage state of the damaged house with 0 to 35% of failed roof tiles and 0 to 5% of failed doors and windows can be defined as no/very minor damage.

According to Eqs. (9)-(12), when the proportion of failed roof tiles is 50% and 90%, it corresponds to two extreme points for the interior damage of the house. Then, when the wind speeds up to 30 m/s, the frequency of the failed roof tiles between 0 and 50% is less than 30%. Therefore, the wind speed when the house located in minor damage level should be lower than 30m/s, which will meet the principle that the exceeding probability does not exceed20% for each damage level. At this time, the failure interval of roof panel can take the value of [0, 10%], the failure interval of doors and windows can take the value of [10%, 25%], and the failure probability of the main load-bearing structure, in that case, will not exceed 12% (Fig. 17).

An important distinguishing point between moderate damage and severe damage is whether the internal loss of the house reaches the maximum value. Therefore, for the states of moderate damage, the failed ratio of roof tiles located in [50%, 90%], the failed ratio of roof panels located in [10%, 30%] and the failed ratio of doors and windows located in [30%, 50%] basically meet the selection principle that the exceeding probability does not exceed 20%. The failure probability of the main load-bearing structure will not exceed 50% at this time. Finally, the definition of each damage level and the division of each component interval are shown in Table 6.

6. Typhoon disaster management system

It is practical significant to carry on the risk analysis of wind disaster and the loss assessment of the low-rise residential buildings, but the more important is to apply the methodology to practice. Based on that, combined the advantage of ArcGIS in geographic information data processing and VB language in interface operation, Typhoon Disaster Management System is developed to predict and assess the loss of group residential buildings under wind hazard.

In order to describe the function of the system in more detail, one field research village located in the southeastern China is took as the object (Fig. 18). This village consists of 550 buildings, and most of them are no more than three floors. The mainly structure types are masonry structures

Table 6 Wind-induced damage level classification of low-rise buildings

Damage state	Qualitative damage description	Roof tiles failure	Roof panels failure	Windows & doors Failure	Main load-bearing structure failure
No/ very minor damage	The roof structure is only slightly damaged on roof tiles. Roof panels, windows and doors are almost intact. The main structure is intact and can continue to be used without repair.	< 35%	0	< 5%	0
Minor damage	Part of roof tiles are damaged, the doors and windows start to break, causing the rain to begin to penetrate, the roof panels are almost intact, the main structure is almost intact, which means the house needs no repair or a little repair.	≥ 35% and < 50%	> 0 and < 10%	≥ 5% and < 25%	> 0 and <12%
Moderate damage	The roof tiles are seriously damaged, the doors and windows are partly destroyed, and the roof panel begins to be damaged, resulting in serious rainwater penetration and internal damage. Local cracks appear in the main load-bearing structure, which means the house needs normal repairs.	≥ 50% and < 90%	≥ 10% and < 30%	≥ 25% and < 50%	≥ 12% and < 50%
Severe damage	The roof structure is completely damaged, the doors and windows are seriously damaged, causing serious rainwater penetration, the main load-bearing structure is destroyed. The structure is about to collapse or has collapsed, and the house is difficult to repair.	≥ 90%	≥ 30%	≥ 50%	≥ 50%

Fig. 21 Buildings information display

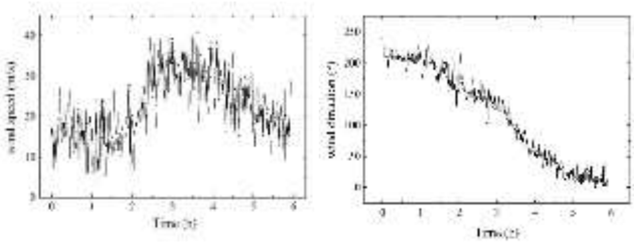

(a) Wind speed (b) Wind direction

Fig. 22 Typhoon Meranti record

Fig. 23 Distribution of damage level for the buildings group

Fig. 24 Distribution of economic loss for the buildings group

(occupied about 38.5%, mainly distributed in the south and southeast), brick-concrete structures (occupied about 44.9%, mainly distributed in the west) and frame structures (occupied about 13.5%, mainly distributed in the north). Besides, half of the building in this village are well conserved, while there are also some buildings in poor conservation, especially for the masonry buildings.

Additionally, the geographic information file also consists the building information like the base area, location, orientation, roof type, number of windows and doors.

First, the file reading function can read the geographic files in three formats (*.shp, *.mxd, *.lyr) containing the corresponding building information. The upper left window can show each layer, and the lower left window is the eagle eye map function and the village map can be displayed in the right window. The information contained in the geographic file can be viewed through a list view or a map display as shown in Fig. 21.

Next, input the typhoon load information. This simulation takes the measured Morandi typhoon record as an example to simulate the loss of the buildings in the village in wind hazard. At 14:00 on September 10, 2016, Moranti was formed on the Pacific Northwest. On September 15th, it landed in Xiamen City (Fujian Province, China). At the time of landing, the center maximum wind power was 48 m/s. For the wind direction, 0° represents the north, and the clockwise is positive. The wind direction and wind speed time history are shown in Fig. 22, where the maximum 10 minutes averaged wind speed is 40.8 m/s at 10 m height and duration time of 6 h.

Thirdly, calculate the building density. Taking the target building center as the circle center and 50 m as the radius, the ratio of the area sum of all buildings inside the circle to the area of the circle is the building density of the target building. Finally, click on Building loss - Start Analysis, the damage level and direct economic loss for each building

Table 7 Damage statistics after typhoon in some counties and cities

Time	Typhoon	Maximum speed	Statistics range	Economics loss (¥)	Data source
2006.8	Saomai	50 m/s	435 thousand people affected and 351.2 thousand buildings broken in Fuding County in Fujian Province	3.28 billion	Fuding County Civil Affairs Bureau
2015.7	Chan-hom	45 m/s	50 thousand people affected in Shangyu District in Zhejiang Province	150 million	Shaoxing City Civil Affairs Bureau
2015.8	Soudelor	35 m/s	More than 30 villages affected in Huoshan County in Anhui Province	450 million	Liuan City Civil Affairs Bureau

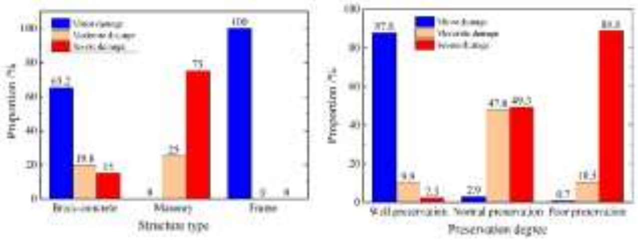

(a) By structure type (b) By preservation degree

Fig. 25 Damage state statistics

after the typhoon can be calculated. The damage states of each building can be displayed in different colors as shown in Fig. 23.

After the wind disaster passed, the economic loss of each building refers to the construction price required to repair the damaged house and restore the same scale and standard before the accident based on the current price. The total economic loss of this village is about 17.43 million ¥, i.e., 2.53 million dollars.

To date, typhoon disaster statistics are often counted by provinces and cities as statistical units, and district/county units are few. Moreover, there are almost no statistics by village units, so it is impossible to compare the simulation results of this village with other typhoon disaster case.

Table 7 lists the disaster statistics of surrounding counties and cities affected by the typhoon disaster in Fujian Province in recent years. Because there are many factors affecting economic losses, such as regional GDP and building density, economic losses in different regions may vary greatly even when the same typhoon passes. Compared with the actual damage statistics, it can be found that the simulation results in this study are generally in line with expectations.

In addition, the system has certain data analysis ability. For example, users can separately count the number of buildings with various damage states according to the structure type, roof type, preservation degree, and the number of building floors. Fig. 25 shows the damage state statistics by structure type and preservation degree respectively, which indicates buildings with masonry structure type and poor preservation surfers more serious damage than other buildings, in other words, these buildings need more reinforcement as expected.

7. Conclusions

In this study, a methodology to predict and assess the loss of group low-rise residential buildings under wind hazard is proposed. Taking into account the structural type, preservation degree, building density, and other influencing factors, the damage matrices concerning wind speed and direction are established for the building envelope structure and the main load-bearing structure respectively. Then, different damage states are defined for the damaged buildings quantitatively and qualitatively. Finally, to apply the damage model and the loss assessment method to reality, Typhoon Management System is established based on the secondary development of ArcGIS.

The simulation results reveal that the order of difficulty of the failure of the three envelope components is: roof panel > doors and windows > roof tiles. Therefore, residenters can use cement tiles or asphalt roof tiles with large weight and beautiful appearance on the roof, which can enhance the wind resistance of roof tiles and roof panels in negative wind pressure areas, and indirectly reduce the probability of door and window being damaged by wind-induced debris.

Additionally, the buildings group in lower building density are more vulnerable to higher damage states compared with the buildings group in higher building density. That would be helpful for the government and building design department to plan the arrangement and layout of the group low-rise residential buildings based on actual conditions.

Finally, combined the advantage of ArcGIS in geographic information data processing and VB language in interface operation, Typhoon Management System can achieve the functions of damage level division and economic loss assessment for group residential buildings during wind disaster. Buildings with field research in Yunmei village were taken as the research target, which verified the feasibility of system and building loss assessment methods.

Acknowledgments

The authors gratefully appreciate the supports by National Key Research and Development Program of China (Grant No. 2018YFD1100405), National Science & Technology Pillar Program during the Twelfth Five-year Plan Period of China (Grant No. 2014BAL05B03).

References

Bhinderwala, S. (1995), *Insurance Loss Analysis of Single Family Dwellings Damaged in Hurricane Andrew*, Clemson University.

Dao, T.N., van de Lindt, J.W., Prevatt, D.O. and Gupta, R. (2012), "Probabilistic procedure for wood-frame roof sheathing panel debris impact to windows in hurricanes", *Eng. Struct.*, **35** 178-187. https://doi.org/10.1016/j.engstruct.2011.11.009.

FEMA (2017), *HAZUS-MH 2.1 technical manual*,

Feng, R., Liu, F., Cai, Q., Yang, G. and Leng, J. (2018), "Field measurements of wind pressure on an open roof during Typhoons HaiKui and SuLi", *Wind Struct.*,**26**(1), 11-24. https://doi.org/10.12989/was.2018.26.1.011.

Huang, P., Tao, L., Quan, Y. and Gu, M. (2010), "Investigation of wind resistance performance of rural house in coastal areas of Zhejiang Province", *J. Catast.,* **25**(4), 90-95.

Huang, Y. and Gu, M. (2018), "Wind-induced responses of supertall buildings considering soil-structure interaction", *Wind Struct.*, **27**(4), 223-234. https://doi.org/10.12989/was.2018.27.4.223.

Li, M. and Wang, G. (2018), "Research on the loss of group residential buildings under fierce winds", *Natural Hazards*, **90**(2), 705-733. https://doi.org/10.1007/s11069-017-3066-1.

Lin, L., Ang, A.H.S., Xia, D.-d., Hu, H.-t., Wang, H.-f. and He, F.-q. (2017), "Fluctuating wind field analysis based on random Fourier spectrum for wind induced response of high-rise structures", *Struct. Eng, Mech., Int. J.*, **63**(6), 837-846. https://doi.org/10.12989/sem.2017.63.6.837.

Lin, N. and Vanmarcke, E. (2010), “Windborne debris risk analysis - Part I. Introduction and methodology”, *Wind Struct., Int. J.*, **13**(2), 191-206.

Liu, X. (2016), *The resistance analysis of low-rise buildings in strong wind*, Dalian University of Technology.

Long, P. (2008), *Study on typhoon vulnerability assessment for civil engineering structures*, Harbin Institute of Technology.

Masters, F. and Gurley, K.R. (2003), “Non-Gaussian simulation: Cumulative distribution function map-based spectral correction”, *J. Eng. Mech.-Asce*. **129**(12), 1418-1428. https://doi.org/10.1061/(ASCE)0733-9399(2003)129:12(1418).

Mitsuta, Y., Fujii, T. and Nagashima, I. (1996). “A Predicting Method of Typhoon Wind Damages”. *Probabi. Mech, Struct. Reliabi.,* **1996***,* 970-973.

Peng, X., Rouche, D.B., Prevatt, D.O. and Gurley, K.R. (2016), *An Engineering-Based Approach to Predict Tornado-Induced Damage*, Springer, Berlin, Germany.

Peng, X.L., Yang, L.P., Gavanski, E., Gurley, K. and Prevatt, D. (2014), “A comparison of methods to estimate peak wind loads on buildings”, *J. Wind Eng. Indust. Aerod*. **126** 11-23. https://doi.org/10.1016/j.jweia.2013.12.013.

Pinelli, J.P., Gurley, K.R., Subramanian, C.S., Hamid, S.S. and Pita, G.L. (2008), “Validation of a probabilistic model for hurricane insurance loss projections in Florida”, *Reliabi. Eng Sys. Safety*. **93**(12), 1896-1905. https://doi.org/10.1016/j.ress.2008.03.017.

Pinelli, J.P., Pita, G., Gurley, K., Torkian, B., Hamid, S. and Subramanian, C. (2011), “Damage Characterization: Application to Florida Public Hurricane Loss Model”, *Natur. Haz. Rev*., **12**(4), 190-195.

Pinelli, J.P., Simiu, E., Gurley, K., Subramanian, C., Zhang, L., Cope, A., Filliben, J.J. and Hamid, S. (2004), “Hurricane damage prediction model for residential structures”, *J. Strut. Eng.-Asce*., **130**(11), 1685-1691. https://doi.org/10.1061/(ASCE)0733-9445(2004)130:11(1685)

Pita, G.L., Pinelli, J.-P., Gurley, K.R. and Hamid, S. (2013), “Hurricane vulnerability modeling: Development and future trends”, *J. Wind Eng. Indust. Aerod.*, **114** 96-105. https://doi.org/10.1016/j.jweia.2012.12.004.

Tachikawa, M. (1983), “Trajectories of flat plates in uniform flow with application to wind-generated missiles”, *J. Wind Eng. Indust. Aerod.*, **14**(1), 443-453. https://doi.org/10.1016/0167-6105(83)90045-4.

TPU (2007), *Aerodynamic database for non-isolated low-rise buildings*, Tokyo Polytechnic University.

Vickery, P.J., Skerlj, P.F., Lin, J., Jr, L.A.T., Young, M.A. and Lavelle, F.M. (2006), “HAZUS-MH Hurricane Model Methodology. II: Damage and Loss Estimation”, *Natur. Haz. Rev*., **7**(2), 94-103. https://doi.org/10.1061/(ASCE)1527-6988(2006)7:2(94).

Wang, D., Chen, X., Li, J. and Cheng, H. (2016), “Wind load characteristics of large billboard structures with two-plate and three-plate configurations”, *Wind Struct*. *Int*. *J*., **22**(6), 703-721. https://doi.org/10.12989/was.2016.22.6.703.

Wang, Y. and Li, Q.S. (2015), “Wind pressure characteristics of a low-rise building with various openings on a roof corner”, *Wind Struct*. *Int*. *J*., **21**(1), 1-23. https://doi.org/10.12989/was.2015.21.1.001.

Yang, L. and Gurley, K.R. (2015), “Efficient stationary multivariate non-Gaussian simulation based on a Hermite PDF model”, *Probabi. Eng. Mech*., **42**(4), 31-41. https://doi.org/10.1016/j.probengmech.2015.09.006.

Zhang, S., Nishijima, K. and Maruyama, T. (2014), “Reliability-based modeling of typhoon induced wind vulnerability for residential buildings in Japan”, *J. Wind Eng. Indust. Aerod*., **124** 68-81. https://doi.org/10.1016/j.jweia.2013.11.004.

Zhong, X., Fang, W. and Cao, S. (2017), “Probabilistic component-based Monte Carlo simulation of vulnerability for a typical low-rise rural residential building in coastal China”, *J. Beijing Normal University (Natural Science)*, **53**(1), 51-59.

AD